Available online at www.sciencedirect.com
ScienceDirect
Computer Physics Communications 177 (2007) 707–719
Computer Physics Communications
www.elsevier.com/locate/cpc

Adaptive continuation algorithms for computing energy levels of rotating Bose–Einstein condensates

S.-L. Chang [a], C.-S. Chien [b,*]

[a] *Center for General Education, Southern Taiwan University, Tainan 710, Taiwan*
[b] *Department of Applied Mathematics, National Chung Hsing University, Taichung 402, Taiwan*

Received 29 March 2007; received in revised form 1 June 2007; accepted 20 June 2007

Available online 28 June 2007

Abstract

We describe adaptive continuation algorithms for computing energy levels of the Bose–Einstein condensates (BEC) with emphasis on the rotating BEC. We show that the rotating BEC in the complex plane is governed by special two-coupled nonlinear Schrödinger equations (NLS) in the real domain, which makes the eigenvalues of the discrete coefficient matrix at least double. A predictor–corrector continuation method is used to trace solution curves of the rotating BEC defined in square domains. The wave functions of the rotating BEC can be easily obtained whenever the solution curves of the two-coupled NLS are numerically traced. From the physical point of view, the proposed algorithm has the advantage that the energy levels of the system are computed intuitively, where the energy information of the associated Schrödinger eigenvalue problem is fully exploited. The superfluid density we obtain on the first solution branch resembles the figure shown in [J.R. Anglin, W. Ketterle, Nature 416 (2002) 211]. We also obtain superfluid densities on the other solution branches, which to the best of our knowledge, have never shown up in the literatures.

Keywords: Nonlinear Schrödinger equation; Angular momentum; Bifurcation; Finite difference method; Adaptive continuation method

1. Introduction

The Bose–Einstein condensates (BEC) obtained by experiments [1], are clouds of ultracold, weakly interacting alkali-metal atoms that occupy a single quantum state, which offer the possibility of investigating superfluidity in the weak-coupling regime [2]. In this paper, we study numerical methods for computing energy levels of a rotating BEC [2,3]. Assume that the rotation is around the z-axis, the governing equation is described by the nonlinear Schrödinger equation (NLS), or the so-called Gross–Pitaevskii equation (GPE) [4,5],

$$\begin{aligned} &\mathbf{i}\epsilon\Psi_t = -\frac{\epsilon^2}{2}\triangle\Psi + V(\mathbf{x})\Psi + \mu|\Psi|^2\Psi - \epsilon\omega L_z\Psi, \quad t > 0,\ \mathbf{x}\in\Omega, \\ &\Psi(\mathbf{x},t) = 0, \quad \mathbf{x}\in\partial\Omega,\ t \geqslant 0. \end{aligned} \tag{1.1}$$

Here $\Psi = \Psi(\mathbf{x},t)$ is the marcoscopic wave function of the BEC, $V(\mathbf{x}) = \frac{1}{2}(\gamma_x^2x^2 + \gamma_y^2y^2 + \gamma_z^2z^2)$ the trapping potential with γ_x, γ_y and γ_z as the trap frequencies in x-, y-, and z-direction, respectively, ϵ a positive constant, $\Omega \subset \mathbf{R}^3$ a bounded domain with piecewise smooth boundary $\partial\Omega$, ω an angular velocity and

$$L_z = xp_y - yp_x = -\mathbf{i}(x\partial y - y\partial x) \tag{1.2}$$

* Corresponding author. Supported by the National Science Council of R.O.C. (Taiwan) through project NSC 95-2115-M005-004-MY3.
E-mail addresses: slchang@mail.stut.edu.tw (S.-L. Chang), cschien@amath.nchu.edu.tw (C.-S. Chien).

0010-4655/$ – see front matter
doi:10.1016/j.cpc.2007.06.009

the z-component of the angular momentum $L = \mathbf{x} \times P$ with the momentum operator $P = -\mathbf{i}\nabla = (p_x, p_y, p_z)^{\mathrm{T}}$. The trapping potential is isotropic if $\gamma_x = \gamma_y = \gamma_z$. When $\epsilon = \mathrm{O}(1)$, Eq. (1.1) describes a weakly interacting condensate. On the other hand, Eq. (1.1) corresponds to a strongly interacting condensate if $\epsilon = \mathrm{o}(1)$. An important invariant of the NLS is the mass conservation constraint, or the normalization of the wave function

$$\int_{\Omega} \left|\Psi(\mathbf{x}, t)\right|^2 \mathrm{d}\mathbf{x} = 1, \quad t \geqslant 0. \tag{1.3}$$

The energy functional associated with (1.1) is

$$E_\mu(\Psi) = \int_{\Omega} \left[\frac{\epsilon^2}{2}\left|\nabla\Psi(\mathbf{x}, t)\right|^2 + V(\mathbf{x})\left|\Psi(\mathbf{x}, t)\right|^2 + \frac{\mu}{2}\left|\Psi(\mathbf{x}, t)\right|^4 - \epsilon\omega\Psi^* L_z\Psi\right]\mathrm{d}\mathbf{x}, \quad t \geqslant 0, \tag{1.4}$$

where Ψ^* denotes the conjugate of Ψ.

The study of quantized vortices in a BEC is of basic importance, which can be obtained in physical experiments. See, e.g., [3,6–9]. Specifically, the vortex lattices of rotating BECs is obtained by setting, e.g., the Na condensate in rotation by rotating laser beams [10]. When the temperatures T are much smaller than the critical temperature T_c, a BEC in a rotational frame is described by the marcoscopic wave function $\Psi(\mathbf{x}, t)$ whose evolution is governed by the NLS with an angular momentum term. In a series of papers [11–13] García-Ripoll and Pérez-García studied the stability of axially symmetric vortex lines, the generation of vortices, and the structure of the ground-state of (1.1). To find the ground-state of (1.1), the same authors [14] exploited a version of the continuous steepest gradient, the so-called imaginary time evolution, to minimize (1.4) by using the Sobolev gradient of the energy functional as the preconditioner. Aftalion and Riviere [15] studied vortex energy and vortex bending for a BEC in a rotating trap. In [16] Aftalion and Du investigated asymptotically and numerically ground state, critical angular velocities and energy diagrams of the rotating BEC in the Thomas–Fermi or semiclassical regime. Recently, Bao et al. [17] studied ground, symmetric and central vortex states as well as their energy and chemical potential diagrams in a rotating BEC. Chin and Krotscheck [18] described a fourth-order algorithm for solving the imaginary time GPE in a rotating anisotropic trap.

To find the wave functions of (1.1), we use the formula

$$\Psi(\mathbf{x}, t) = e^{-\mathbf{i}\lambda t/\epsilon}\mathbf{v}(\mathbf{x}), \tag{1.5}$$

where λ is the chemical potential of the condensate, and $\mathbf{v}(\mathbf{x})$ a complex function independent of t. Note that the chemical potential λ is proportional to the total energy of the system. Substituting (1.5) into (1.1), we obtain the associated nonlinear eigenvalue problem

$$\begin{aligned} &\lambda\mathbf{v}(\mathbf{x}) = -\frac{\epsilon^2}{2}\triangle\mathbf{v}(\mathbf{x}) + V(\mathbf{x})\mathbf{v}(\mathbf{x}) + \mu\left|\mathbf{v}(\mathbf{x})\right|^2\mathbf{v}(\mathbf{x}) - \epsilon\omega L_z\mathbf{v}(\mathbf{x}), \quad \mathbf{x} \in \Omega, \\ &\mathbf{v}(\mathbf{x}) = 0 \quad \text{on } \partial\Omega. \end{aligned} \tag{1.6}$$

Recently, Chang and Chien [19] and Chang et al. [20,21] investigated stationary state solutions and wave functions of (1.6) using numerical continuation methods, where λ was treated as the continuation parameter. The continuation algorithm [21] can efficiently compute stationary state solutions of (1.6) with mass conservation constraint, where we start with bifurcation points on the trivial solution curve $\{(\mathbf{v}, \lambda) = (0, \lambda) \mid \lambda \in \mathbf{R}\}$. The constraint

$$\int_{\Omega} \left|\mathbf{v}(x)\right|^2 \mathrm{d}\mathbf{x} = 1 \tag{1.7}$$

is regarded as a target point on the nontrivial solution curve. The wave function $\Psi(\mathbf{x}, t)$ can be easily obtained using (1.5) whenever the target point on the solution curve is reached.

Among the many states of the BEC, probably the ground state solution with peak in the central part of the domain Ω is of special interest [10,22], where the probability density of the wave function is relatively small in the other part of Ω. Actually, the peak solution is formed step by step in the continuation process. This suggests that we may use adaptive grids on Ω in the continuation algorithm. The idea of adaptive mesh refinement is well known in finite element methods. We refer to [23] for the application to continuation methods.

In this paper, we will describe an adaptive continuation algorithm for computing energy levels and wave functions of the GPE with emphasis on (1.1). Of particular interest is the investigation of the ground-state and the first excited state solutions. Since $\mathbf{v}(\mathbf{x})$ is a complex function, it can be expressed as $\mathbf{v}(\mathbf{x}) = v_1(\mathbf{x}) + \mathbf{i}v_2(\mathbf{x})$, where $v_1(\mathbf{x})$ and $v_2(\mathbf{x})$ are two real functions. Then we decompose (1.6) into two-coupled nonlinear Schrödinger equations. Next, we detect bifurcation points along the trivial solution curve $\{(0, \lambda) \mid \lambda \in \mathbf{R}\}$. The bifurcation point will be used as an initial guess for computing an energy level and a stationary state solution of (1.6), where the continuation method is used as an iterative method for curve-tracking. Using the process described

above, we will obtain the energy level as well as the wave function of (1.1). By comparing our numerical results with those in [17], the wave function we obtain at the target point of the first solution branch is indeed the ground-state solution of the rotating BEC.

This paper is organized as follows. In Section 2 we discuss the relationship between energy levels and eigenvalues of the Schrödinger eigenvalue problem (SEP), and the corresponding bifurcations of a NLS. Furthermore, we address how the energy levels are affected by the angular momentum and the spin of a particle. In Section 3, we decompose the rotating GPE into two-coupled nonlinear GPEs in the real domain. We also discuss how to use a predictor–corrector continuation method to trace solution curves of the GPE. In Section 4, we discuss centered difference approximations for the rotating BEC defined on the unit square. We show that the locations of bifurcations of the GPE are affected by the angular momentum. We also give a comparison between spectral-Galerkin methods and centered difference approximations in the context of continuation methods for curve-tracking. In Section 5 we describe an adaptive continuation algorithm for computing wave functions of (1.6). The proposed algorithm also can be used to compute solution curves of certain reaction-diffusion systems, which might have multiple interior/boundary peak solutions [24,25]. Our numerical results reported in Section 6 show that the ground-state superfluid density of the rotating BEC resemble the figure shown in [10] if the length of the domain is large enough. Moreover, we obtain superfluid densities on the other solution branches of the rotating BEC, which to the best of our knowledge, have never shown up in published literatures. Finally, some conclusions are given in Section 7.

2. Energy, eigenvalue and bifurcation

We will show that the minimum eigenvalue of the linear Schrödinger equation corresponds to the first bifurcation of the NLS. To start with, we consider the 1D. Schrödinger equation

$$\begin{aligned} &\phi''(x) = \frac{2M}{\hbar^2}\big[V(x) - E\big]\phi(x), \quad x \in (0,a),\\ &\phi(0) = \phi(a) = 0, \end{aligned} \tag{2.1}$$

where M is the mass of a quantum particle, $\hbar$ Planck's constant, E the total energy, and $V(x)$ the potential energy, which has the following form

$$V(x) = \frac{1}{2}\alpha x^2 \tag{2.2}$$

for some constant $\alpha > 0$. If we set $V(x) = 0$ in (2.1), then the Schrödinger equation reduces to

$$\begin{aligned} &\phi''(x) = -k^2\phi(x) \equiv -\lambda\phi(x), \quad x \in (0,a),\\ &\phi(0) = \phi(a) = 0, \end{aligned} \tag{2.3}$$

where $k = \frac{\sqrt{2ME}}{\hbar}$. Eq. (2.3) is a linear eigenvalue problem with eigenpairs

$$\begin{aligned} &k^2 = \lambda_n = \frac{n^2\pi^2}{a^2},\\ &u_n(x) = \sin\left(n\pi\frac{x}{a}\right), \quad n = 1,2,3,\ldots. \end{aligned} \tag{2.4}$$

From (2.4) we have $k = \frac{n\pi}{a}$ and so the allowed energies for a particle in a 1D domain are

$$E_n = \frac{\hbar^2k^2}{2M} = n^2\frac{\pi^2\hbar^2}{2Ma^2}, \quad n = 1,2,3,\ldots. \tag{2.5}$$

Eq. (2.5) shows that the energy of the particle is proportional to the eigenvalue λ_n, and the ground-state energy is obtained when $n = 1$, i.e.,

$$E_1 = \frac{\pi^2\hbar^2}{2Ma^2}. \tag{2.6}$$

Note that every energy level in the 1D case is nondegenerate.

Next, we consider the nonlinear eigenvalue problem

$$\phi''(x) = -\frac{2ME}{\hbar^2}\phi(x) + \phi(x)^3, \tag{2.7}$$

which can be simplified as

$$\phi''(x) = -\lambda\phi(x) + \phi(x)^3. \tag{2.8}$$

It is well known that the bifurcations of (2.8) locate at the eigenvalues of (2.3) and nontrivial solution curves of (2.8) will bifurcate there.

The 2D generalization of (2.1) with $V(\mathbf{x}) = 0$ is

$$\begin{aligned} &\triangle\phi(\mathbf{x}) = -k^2\phi(\mathbf{x}) \equiv -\lambda\phi(\mathbf{x}), \quad \mathbf{x} \in \Omega = (0,a)^2, \\ &\phi(\mathbf{x}) = 0 \quad \text{on } \partial\Omega, \end{aligned} \tag{2.9}$$

where $k^2 = \frac{2ME}{\hbar^2}$. The eigenpairs of (2.9) are

$$\begin{aligned} &k^2 = \lambda_{m,n} = (m^2+n^2)\frac{\pi^2}{a^2}, \\ &\phi_{m,n}(x,y) = \sin\frac{m\pi x}{a}\cdot\sin\frac{n\pi y}{a}, \quad m,n = 1,2,3,\ldots. \end{aligned} \tag{2.10}$$

Thus, the allowed energies for a particle in a 2D domain are

$$E_{m,n} = \frac{k^2\hbar^2}{2M} = (m^2+n^2)\frac{\pi^2\hbar^2}{2Ma^2}, \quad m,n = 1,2,3,\ldots. \tag{2.11}$$

Note that the energy levels $E_{n,n}$ are nondegenerate for $n = 1,2,3,\ldots$. In particular, the ground-state energy is nondegenerate, while most of the levels $E_{m,n}$ with $m \neq n$ are at least twofold degenerate. For instance, we have $E_{1,8} = E_{8,1} = E_{7,4} = E_{4,7}$, which is fourfold degenerate. Now we impose the trapping potential $V(\mathbf{x})$ in (2.9) and consider

$$\begin{aligned} &\triangle\phi(\mathbf{x}) = \frac{2M}{\hbar^2}\big[V(\mathbf{x}) - E\big]\phi(\mathbf{x}), \quad \mathbf{x} \in \Omega = (0,a)^2, \\ &\phi(\mathbf{x}) = 0 \quad \text{on } \partial\Omega. \end{aligned} \tag{2.12}$$

Eq. (2.12) is also called the Schrödinger eigenvalue problem (SEP). The eigenpairs $(E_{m,n}, \phi_{m,n}(\mathbf{x}))$ can be obtained using certain numerical methods. We may rewrite (2.12) as

$$\begin{aligned} &\left[-\frac{\hbar^2}{2M}\triangle + V(\mathbf{x})\right]\phi(\mathbf{x}) \equiv H\phi(\mathbf{x}) = E\phi(\mathbf{x}), \quad \mathbf{x} \in \Omega, \\ &\phi(\mathbf{x}) = 0 \quad \text{on } \partial\Omega, \end{aligned} \tag{2.13}$$

where H is the Hamiltonian operator, or the energy operator. For a specific eigenpair $(E_{m,n}, \phi_{m,n}(\mathbf{x}))$ we have

$$H\phi_{m,n}(\mathbf{x}) = E_{m,n}\phi_{m,n}(\mathbf{x}), \quad m,n = 1,2,3,\ldots. \tag{2.14}$$

Note that in the discrete case the degeneracy of energy levels of a quantum particle governed by (2.12) will be preserved only if the trapping potential $V(\mathbf{x})$ is isotropic; see [20,21] for details. However, we will see in Section 4 that this property does not hold for rotating BEC. To be precise, the degeneracy of energy levels of a rotating BEC is at least twofold regardless the trapping potential is isotropic or nonisotropic.

We impose the cubic term $|\phi(\mathbf{x})|^2\phi(\mathbf{x})$ in the right-hand side of (2.12) and obtain the NLS

$$\begin{aligned} &\triangle\phi(\mathbf{x}) = \frac{2M}{\hbar^2}\big[V(\mathbf{x}) - E\big]\phi(\mathbf{x}) + \big|\phi(\mathbf{x})\big|^2\phi(\mathbf{x}), \quad \mathbf{x} \in \Omega, \\ &\phi(\mathbf{x}) = 0 \quad \text{on } \partial\Omega. \end{aligned} \tag{2.15}$$

Eq. (2.15) is a nonlinear eigenvalue problem. Nontrivial solution curves of (2.15) will branch at the bifurcation point $(0,\lambda^*)$ on the trivial solution curve $\{(0,\lambda) \mid \lambda \in \mathbf{R}\}$, where λ^* is an eigenvalue of (2.12). In what follows, we will rescale the coefficients of (2.15) and rewrite the NLS in a slightly different way. To study the ground-state as well as other excited state solutions of the rotating BEC, we impose the angular momentum term in (2.15) and obtain the stationary state NLS

$$\begin{aligned} &\frac{\varepsilon^2}{2}\triangle\phi(\mathbf{x}) = V(\mathbf{x})\phi(\mathbf{x}) - \lambda\phi(\mathbf{x}) + \mu\big|\phi(\mathbf{x})\big|^2\phi(\mathbf{x}) - \varepsilon\omega L_z\phi(\mathbf{x}), \quad \mathbf{x} \in \Omega, \\ &\phi(\mathbf{x}) = 0 \quad \text{on } \partial\Omega. \end{aligned} \tag{2.16}$$

In conclusion, to compute the ground-state solution of (2.15), it suffices to use the minimum eigenvalue of (2.12) corresponding to the ground-state energy as an initial guess for the parameter variable. More precisely, we use the first bifurcation point of (2.15) as an initial guess for computing the ground-state solution. The other exercised state solutions of (2.15) can be treated in a similar way. The above-mentioned discussion also works for the GPE with angular momentum term. We remark here that the locations of bifurcations of (2.16) are different from those of (2.15) because of the affect of the angular momentum. We will discuss how to use a predictor–corrector continuation method to trace the solution curve branching from the first bifurcation of the rotating BEC until the mass conservation constraint is satisfied.

3. Continuation for energy levels

Let $\mathbf{v}(\mathbf{x}) = v_1(\mathbf{x}) + \mathbf{i}v_2(\mathbf{x})$ in (1.6), where $v_1(\mathbf{x})$ and $v_2(\mathbf{x})$ are two real functions. The real and imaginary parts of (1.6) are

$$\lambda v_1(\mathbf{x}) = -\frac{\varepsilon^2}{2}\triangle v_1(\mathbf{x}) + V(\mathbf{x})v_1(\mathbf{x}) + \mu\big|\mathbf{v}(\mathbf{x})\big|^2 v_1(\mathbf{x}) - \varepsilon\omega(x\partial y - y\partial x)v_2(\mathbf{x}), \tag{3.1}$$

$$\lambda v_2(\mathbf{x}) = -\frac{\varepsilon^2}{2}\triangle v_2(\mathbf{x}) + V(\mathbf{x})v_2(\mathbf{x}) + \mu\big|\mathbf{v}(\mathbf{x})\big|^2 v_2(\mathbf{x}) + \varepsilon\omega(x\partial y - y\partial x)v_1(\mathbf{x}), \tag{3.2}$$

respectively. Eqs. (3.1) and (3.2) are special two-coupled NLS equations where we have the same chemical potential λ for both equations. The mass conservation constraint for the system is

$$\int_{\Omega} |\mathbf{v}|^2 \,\mathrm{d}\mathbf{x} = 1, \tag{3.3}$$

where $|\mathbf{v}|^2 = v_1^2 + v_2^2$. One can easily verify that the Cauchy–Riemann equations does not hold for (3.1) and (3.2).

We rewrite (3.1) and (3.2) as

$$-\frac{\varepsilon^2}{2}\triangle v_1(\mathbf{x}) - \lambda v_1(\mathbf{x}) + V(\mathbf{x})v_1(\mathbf{x}) + \mu\big|\mathbf{v}(\mathbf{x})\big|^2 v_1(\mathbf{x}) - \varepsilon\omega(x\partial y - y\partial x)v_2(\mathbf{x}) = 0, \tag{3.4}$$

$$-\frac{\varepsilon^2}{2}\triangle v_2(\mathbf{x}) - \lambda v_2(\mathbf{x}) + V(\mathbf{x})v_2(\mathbf{x}) + \mu\big|\mathbf{v}(\mathbf{x})\big|^2 v_2(\mathbf{x}) + \varepsilon\omega(x\partial y - y\partial x)v_1(\mathbf{x}) = 0. \tag{3.5}$$

Eqs. (3.4) and (3.5) constitute a system of parameter-dependent operator equations of the following form

$$F(\mathbf{v}, \lambda, \mu) = 0. \tag{3.6}$$

We treat the chemical potential λ as the continuation parameter [19,20], and keep the parameter μ fixed. Then (3.6) can be simplified as

$$F(\mathbf{v}, \lambda) = 0. \tag{3.7}$$

Note that if we neglect the angular momentum terms in (3.4) and (3.5), then the bifurcations of (3.7) will locate at the eigenvalues of the Schrödinger eigenvalue problem

$$-\frac{\varepsilon^2}{2}\triangle v_i(\mathbf{x}) - \lambda v_i(\mathbf{x}) + V(\mathbf{x})v_i(\mathbf{x}) = 0, \quad i = 1, 2. \tag{3.8}$$

Assume that the trapping potential is $V(\mathbf{x}) = \frac{1}{2}(x^2 + \gamma_y^2 y^2)$. In the case of a weakly interacting condensate, Bao et al. [22] proposed to use the ground-state solution of (3.8), namely,

$$\lambda_g = \left(\frac{1+\gamma_y}{2}\right)\varepsilon, \qquad (v_i)_g(\mathbf{x}) = \frac{\gamma_y^{1/4}}{(\pi\varepsilon)^{1/2}}\exp\big(-(x^2 + \gamma_y y^2)/2\varepsilon\big), \quad i = 1, 2, \tag{3.9}$$

as an approximate ground-state solution of the GPE. On the other hand, Chang et al. [21] used the bifurcation points on the trivial solution curve $\{(\mathbf{v}, \lambda) = (0, \lambda) \mid \lambda \in \mathbf{R}\}$ of the GPE as an initial guess to computing wave functions. In this paper, we will exploit the technique discussed in Section 2. In practice, the continuation method can be regarded as an iterative method for computing wave functions of the GPE. We start with the first bifurcation point $(\mathbf{v}, \lambda) = (0, \lambda^*)$ on the trivial solution curve. The value λ^* supplies us with the minimum chemical potential for the system. The continuation method updates both the stationary state $\mathbf{v}$ and the chemical potential λ simultaneously until the mass conservation constraint is satisfied. That is, there is only one target point on the first solution branch of (3.7) which satisfies (3.3). From the viewpoint of bifurcation the idea of minimum chemical potential is similar to that of the external load in a buckling problem in mechanics. When the external load λ is greater than a critical value λ^* of a plate, which is the location of the first bifurcation point, the buckling phenomenon will occur in the plate. The target points on the other solution branches of (3.7) corresponding to excited state solutions of the system can be treated in a similar way. By comparing our numerical results with those in [17], the wave function at the target point of the first solution branch is indeed the ground-state solution of the rotating BEC.

It is well known that the bifurcations of the GPE are pitchfork. See, e.g., [20]. The pitchfork bifurcation can be supercritical or subcritical depending on the coefficient μ is positive or negative. Note that the locations of bifurcations of the rotating BEC will be different from those of the GPE without angular momentum. This will become evident if we examine the Jacobian matrix associated with the rotating BEC given in Section 4. Now we briefly address how numerical continuation methods can be used to compute wave functions of (1.1). The discretizations of (3.1) and (3.2) are a nonlinear system of equations. Assume that a point $\mathbf{y}_i = (\mathbf{v}_i, \lambda_i)$ on a solution curve c of the system has been accepted as an approximating point. A new point $\mathbf{z}_{i+1,1}$ is predicted, say,

using the Euler predictor

$$\mathbf{z}_{i+1,1} = \mathbf{y}_i + \delta_i \mathbf{w}_i,$$

where $\mathbf{w}_i$ is the unit tangent vector yet to be determined, and $\delta_i > 0$ is the steplength. In the corrector step we perform Newton's method to improve the accuracy of the approximating point $\mathbf{y}_i$. By imposing the constraint (3.3) on the discrete nonlinear system, we only have one target point, say, on the first solution curve of (1.1). Therefore, the stepsize in the predicted step of the continuation method can be chosen as large as possible. We stop the continuation process whenever the target point is reached. The wave function can be computed via the formula (1.5) for any time scale t. That is,

$$\Psi(\mathbf{x}, t) = e^{-\mathbf{i}\lambda t/\varepsilon}\mathbf{v}(\mathbf{x}) = e^{-\mathbf{i}\lambda t/\varepsilon}\big(v_1(\mathbf{x}) + \mathbf{i}v_2(\mathbf{x})\big). \tag{3.10}$$

Similar ideas have been used in [21] to compute wave functions of two- and three-coupled NLS.

4. The rotating BEC on a square

4.1. Centered difference approximations

We consider the nonlinear eigenvalue problem (1.6) defined on the unit cube $(0, 1)^3$, where the angular momentum in the z-direction L_z is defined as in (1.2). The governing equation for the rotating BEC is confined on the unit square $\Omega = (0, 1)^2$. For convenience we let $v(\mathbf{x}) = R(\mathbf{x}) + \mathbf{i}T(\mathbf{x})$, where $R(\mathbf{x})$ and $T(\mathbf{x})$ are two real functions with $\mathbf{x} = (x, y)^{\mathrm{T}} \in \Omega$. The real and imaginary parts of (1.6) with $\varepsilon = 1$ can be expressed as

$$\begin{aligned}
&-\frac{1}{2}\triangle R - \lambda R + V(\mathbf{x})R + \mu(R^2 + T^2)R + \omega(-xT_y + yT_x) = 0, \\
&-\frac{1}{2}\triangle T - \lambda T + V(\mathbf{x})T + \mu(R^2 + T^2)T + \omega(xR_y - yR_x) = 0, \\
&R(\mathbf{x}) = T(\mathbf{x}) = 0 \quad \text{on } \partial\Omega,
\end{aligned} \qquad \text{in } \Omega = (0, 1)^2, \tag{4.1}$$

where R_x, T_x and R_y, T_y denote the partial derivatives of R and T with respect to x and y, respectively. We discretize (4.1) by using the centered difference approximations with uniform meshsize $h = \frac{1}{N+1}$ on the x- and y-axis. For simplicity we also use R and T to denote the discrete grid functions on Ω. The centered difference analogue of (4.1) is

$$F(R, T, \lambda) = \begin{bmatrix} F_1(R, T, \lambda) \\ F_2(R, T, \lambda) \end{bmatrix} = 0, \tag{4.2}$$

where

$$\begin{aligned}
F_1(R, T, \lambda) &= AR + BT - \lambda R + \big(V(\mathbf{x}) + \mu(R \circ R + T \circ T)\big)R = 0, \\
F_2(R, T, \lambda) &= -BR + AT - \lambda T + \big(V(\mathbf{x}) + \mu(R \circ R + T \circ T)\big)T = 0,
\end{aligned} \tag{4.3}$$

with "$\circ$" denotes the Hadamard product, A the coefficient matrix corresponding to the Laplacian $-\frac{1}{2}\triangle$, and

$$B = \begin{bmatrix} y_1 G & -L & & \\ L & y_2 G & \ddots & \\ & \ddots & \ddots & \ddots \\ & & \ddots & \ddots & -L \\ & & & L & y_N G \end{bmatrix} \in \mathbf{R}^{N^2 \times N^2} \quad \text{with } G = \frac{\omega}{h}\begin{bmatrix} 0 & 1 & & \\ -1 & 0 & \ddots & \\ & \ddots & \ddots & \ddots \\ & & \ddots & \ddots & 1 \\ & & & -1 & 0 \end{bmatrix} \in \mathbf{R}^{N \times N}$$

and $L = \frac{\omega}{h}\mathrm{diag}(x_1, \ldots, x_N) \in \mathbf{R}^{N \times N}$. Note that B is skew-symmetric, i.e., $B^{\mathrm{T}} = -B$. Let $W = [R, T]^{\mathrm{T}}$. The Jacobian matrix $DF = [D_W F, D_\lambda F]$ is

$$DF = \begin{bmatrix} A - (\lambda I - V(\mathbf{x})I - \mu(3R^2 + T^2)) & B + 2\mu RT & R \\ -B + 2\mu RT & A - (\lambda I - V(\mathbf{x})I - \mu(R^2 + 3T^2)) & T \end{bmatrix}, \tag{4.4}$$

where for convenience we use R^2 and RT to denote the Hadamard products $R \circ R$ and $R \circ T$, respectively. It is clear form (4.4) that the locations of bifurcations of the rotating BEC will be different from those of the two-coupled NLS discussed in [19]. Note that $D_W F$ is the linearization of the mapping F at the equilibrium $W_0 = [0, 0]^{\mathrm{T}}$, i.e.,

$$D_W F(W_0, \lambda) = K - \lambda \begin{bmatrix} I & 0 \\ 0 & I \end{bmatrix}, \tag{4.5}$$

where

$$K = \begin{bmatrix} A + V(\mathbf{x})I & B \\ -B & A + V(\mathbf{x})I \end{bmatrix}. \tag{4.6}$$

Since A is symmetric and B is skew-symmetric, K is a symmetric matrix.

Definition 4.1. A 2×2 block matrix

$$M = \begin{bmatrix} S & U \\ W & S^{\mathrm{T}} \end{bmatrix}, \quad S, U, W \in \mathbf{R}^{n\times n}$$

is called skew-Hamiltonian if $U^{\mathrm{T}} = -U$ and $W^{\mathrm{T}} = -W$, and Hamiltonian if $U^{\mathrm{T}} = U$ and $W^{\mathrm{T}} = W$.

Skew-Hamiltonian/Hamiltonian (SHH) pencils arise in the optimal control problems which lead to quadratic matrix eigenvalue problems. It is clear that the matrix K is skew-Hamiltonian. Let $\rho(\alpha)$ and $\sigma(\alpha)$ denote the geometric multiplicity and the algebraic multiplicity of an eigenvalue α. We have the following result.

Theorem 4.2. *All the eigenvalues of the matrix K are real and at least double.*

Proof. Since K is symmetric, all the eigenvalues are real. Let $[R_1, T_1]^{\mathrm{T}}$ be an eigenvector of K associated with the eigenvalue α. It is clear that $[T_1, -R_1]^{\mathrm{T}}$ is also an eigenvector of K associated with α. Since $\rho(\alpha) \leqslant \sigma(\alpha)$, the result follows immediately. □

Remark 4.3. From the proof of Theorem 4.2 it follows immediately that the two eigenvectors of the matrix K are orthogonal. Since the trapping potential $V(\mathbf{x})$ locates at the diagonal of the matrix K, it shows that the degeneracy is twofold regardless $V(\mathbf{x})$ is isotropic or nonisotropic, which is different from the case of the NLS without angular momentum term; see [20,21] for details.

An interesting property of skew-Hamiltonian pencils is that the eigenvalues are all double. Note that the eigenvalues of K are all double is owing to the fact that we decompose the function $\mathbf{v}$ into real and imaginary parts. In [26] Mehrmann and Watkins proposed a delicate algorithm, the so-called skew-Hamiltonian isotropic implicitly restarted Arnoldi method (SHIRA), which can efficiently compute eigenvectors and invariant subspaces of SHH. To compute eigenpairs of the matrix K using SHIRA is beyond the scope of this paper, and will be given elsewhere.

Remark 4.4. For the GPE without angular momentum, we have $B = O$ in (4.5). In this case, the locations of bifurcations are different from the one with angular momentum. For the latter, the locations of bifurcation will vary with respect to the angular velocity.

The centered difference approximations of the rotating BEC on the unit disk also can be formulated using the polar coordinates, and will be discussed elsewhere. By regarding the conventional finite difference method as a special kind of finite element methods using piecewise bilinear and linear interpolatory functions [27], the superconvergence rate $\mathrm{O}(h^2)$ of solution derivatives in the discrete H_1-norm is derived in [28] using rectangular difference grids for certain parameter-dependent problems, including the NLS with positive solutions.

4.2. Spectral-Galerkin methods

Currently we are developing spectral-Galerkin [29,30] and pseudospectral-Galerkin continuation algorithms for tracing solution curves of parameter-dependent problems, where the trigonometric sine functions in (2.10), the Legendre polynomials and the Chebyshev polynomials are used as the bases functions. Of special interest is the implementation of sine-spectral-Galerkin method, which are the eigenfunctions of the Laplacian in (2.9). The importance of this particular choice of basis functions is twofold:

(i) Let $\{\sin j\pi x \sin k\pi y \mid 1 \leqslant j, k \leqslant N\}$ be the given basis functions. It is straightforward to see that the discrete eigenvalues of (2.9) are exactly the same as those given (2.10).
(ii) In this regard, the linear bifurcation theory is reproduced exactly for certain semilinear linear elliptic eigenvalue problem. As an example, consider

$$\begin{aligned} &\triangle u + \lambda \sinh u = 0 \quad \text{in } \Omega = (0,1)^2, \\ &u = 0 \quad \text{on } \partial\Omega. \end{aligned} \tag{4.7}$$

Eq. (4.7) describes a model for the equilibrium of a set of point vortices or a guiding-center plasma in the domain Ω. If we use the sine-spectral method to discretize (4.7), then the locations of bifurcations of the discrete problem are exactly as those of the continuous problem (4.7). Note that other discretization schemes such as finite difference or finite elements do not reproduce linear theory exactly unless the meshsize $h \to 0$, which is impossible in practical computations. Other basis functions such as Legendre and Chebyshev polynomials do not compute bifurcation points of (4.7) exactly. Therefore, it is expected that the sine-spectral-Galerkin method would compute more accurate energy levels of the SEP (2.13) than the other discretization methods mentioned above. However, all spectral-Galerkin methods will generate full dense matrices even for (2.13). For the computational cost we believe that there is a balance between the number of basis functions used in spectral-Galerkin methods and the meshsize of finite differences or finite elements. A detailed investigation will be given elsewhere.

5. Adaptive continuation algorithms

To compute wave functions of the GPE, in general one has to discretize the left-hand side of (1.1) using, e.g., the Grank–Nicolson finite difference schemes. See, for instance, [22] and the further references cited therein. The numerical scheme described in [21] gives a different approach for computing wave functions of the BEC. Among the many states of the GPE, probably the ground state solution is of special interest, which in general has a peak in the central part of the domain Ω, and the probability density is relatively small in the other part of Ω. Notice that multiple interior or boundary peak solutions also exist in certain reaction-diffusion systems with Neumann boundary conditions [24,25]. This suggests that we can use adaptive grids on Ω if continuation methods are exploited to treat such type of problems.

For convenience we assume that Ω is a square, and we are interested in the peak solution of the problem we wish to solve. The peak of the solution will be formed gradually [19]. Thus we can find the maximum of $\mathbf{v}(\mathbf{x})$ in Ω in each continuation step. Suppose that the maximum of $\mathbf{v}(\mathbf{x})$ is located at $\mathbf{x}^* \in \Omega$. Let $\Omega_1 \subset \Omega$ be a square with center at $\mathbf{x}^*$, and the four corners are $\mathbf{x}_i$, $i = 1{:}4$. If $\mathbf{x}^*$ is indeed the location of the peak, then $\mathbf{v}(\mathbf{x}^*)$ will increase, and $\mathbf{v}(\mathbf{x}_i)$, $i = 1{:}4$, will decrease starting from certain step of the continuation algorithm. Thus we may refine the grid on Ω_1, say every ten continuation steps, and then shrink Ω_1 to a smaller square $\Omega_2 \subset \Omega_1$. We repeat this process until the target point is reached. Recall in continuation methods we always start from the trivial solution near the bifurcation point of the GPE, which is far from the target point we wish to obtain. Therefore, at the beginning of the continuation algorithm we may deploy a coarse grid with meshsize h on Ω.

The adaptive mesh refinement strategy we propose in the context of continuation method is described as follows.

Algorithm 5.1. Adaptive mesh refinement continuation algorithm for reaction-diffusion systems.

Input: $\gamma :=$ accuracy tolerance for the approximating points on the solution curve.
$\lambda :=$ the continuation parameter.
$h :=$ the uniform meshsize on the starting coarse grid.
$h_{\min} :=$ the minimum meshsize.
$j :=$ the index of continuation step.
$j = 1$.

Step 1. Use a predictor–corrector continuation algorithm to find an approximating point on the solution curve, where $\|F(\cdot)\| < \gamma$.

Step 2. Find the global maximum $\mathbf{v}^{(j)}(\mathbf{x}^*)$ and the values $\mathbf{v}^{(j)}(\mathbf{x}_i)$, $i = 1{:}4$, on the four corners of $\Omega_1 \subset \Omega$ with center at $\mathbf{x}^*$.

Step 3. If $j \leqslant J$ for some positive integer J, or if $j > J$ and $h = h_{\min}$, go to Step 4;
Else, determine the increasing and decreasing rates of $\mathbf{v}^{(j)}(\mathbf{x}^*)$ and $\mathbf{v}^{(j)}(\mathbf{x}_i)$, $i = 1{:}4$, respectively, If

$$\frac{\mathbf{v}^{(j-1)}(\mathbf{x}^*) - \mathbf{v}^{(j-2)}(\mathbf{x}^*)}{\mathbf{v}^{(j-2)}(\mathbf{x}^*)} < \frac{\mathbf{v}^{(j)}(\mathbf{x}^*) - \mathbf{v}^{(j-1)}(\mathbf{x}^*)}{\mathbf{v}^{(j-1)}(\mathbf{x}^*)} \quad \text{and}$$

$$\left|\frac{\mathbf{v}^{(j-1)}(\mathbf{x}_i) - \mathbf{v}^{(j-2)}(\mathbf{x}_i)}{\mathbf{v}^{(j-2)}(\mathbf{x}_i)}\right| < \left|\frac{\mathbf{v}^{(j)}(\mathbf{x}_i) - \mathbf{v}^{(j-1)}(\mathbf{x}_i)}{\mathbf{v}^{(j-1)}(\mathbf{x}_i)}\right|, \quad i = 1{:}4,$$

and if $j = 10 \cdot k$, do
(i) refine the grid on Ω_1 with uniform meshsize $\frac{h}{2}$, if $\frac{h}{2} \leqslant h_{\min}$, set $\frac{h}{2} = h_{\min}$;
(ii) replace the corner points $\mathbf{x}_i$, $i = 4$, in Ω_1 by those of a smaller square $\Omega_2 \subset \Omega_1$ with center at $\mathbf{x}^*$;
(iii) construct the coefficient matrix associated with the differential operator;
Else, go to Step 4.

Step 4. Set $j = j + 1$ and go to Step 1 until the target point is reached.

Step 5. Compute $\Psi(\mathbf{x}, t) = e^{-\mathbf{i}\lambda t}\mathbf{v}(\mathbf{x})$.

Remark 5.2. Algorithm 5.1 can be easily modified to compute multiple peak solutions of a reaction-diffusion system.

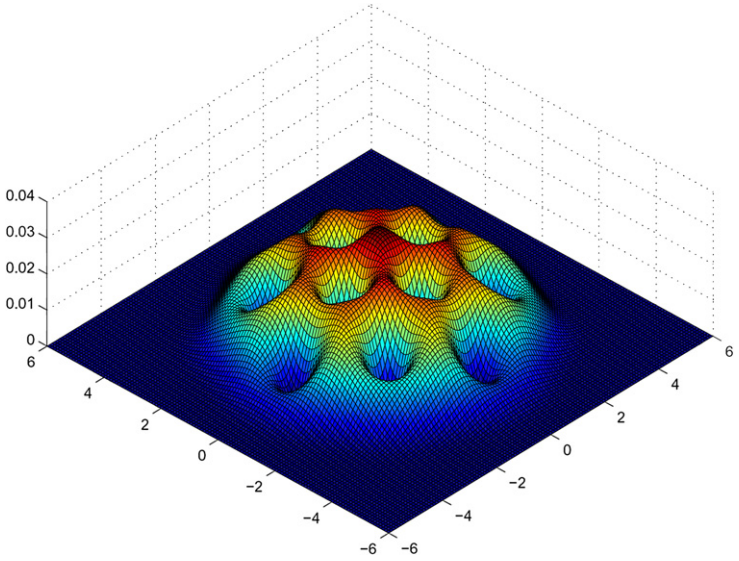

Fig. 1. The contour of the superfluid density $|\mathbf{v}|^2$ on the target point of the first solution branch of Eq. (1.6) with $l = 6$ and $\omega = 0.9$ at $\lambda = 3.6286285$.

In general, Algorithm 5.1 may not work for the higher excited state solutions of the GPE. We recall Algorithm 4.1 in [21], where the target point is obtained on the fine grid $\Omega_{\widetilde{h}}$ using a two-grid discretization scheme. In practice, we do not have to compute approximating points of the solution curve $\widetilde{c}$ on $\Omega_{\widetilde{h}}$ with desired accuracy except the target point. To save the unnecessary computational cost, we propose to trace the solution curve on the coarse grid Ω_h until the target point is reached, where $\widetilde{h} = \mathrm{O}(h^2)$. Then we use this target point as a predicted point to compute its counterpart on $\Omega_{\widetilde{h}}$. In summary, we obtain a simplified two-grid discretization scheme for computing the target on a solution curve of the GPE.

Algorithm 5.3. A simplified two-grid scheme for computing the target point on a solution curve of the GPE.

Input: $\gamma :=$ accuracy tolerance for the approximating points on the solution curve.
Step 1. Outer continuation. Use a predictor–corrector continuation algorithm to compute an approximating points on the coarse grid Ω_h until the target point is reached, where $\|F(\cdot)\| < \gamma$.
Step 2. Compute the target point on the fine grid.
(i) Predictor: Use the target point obtained in Step 1 as the predicted point.
(ii) Corrector. (a) Make a correction on the fine grid; (b) Perform Newton's method until $\|F(\cdot)\| < \gamma$.
Step 3. Compute $\Psi(\mathbf{x}, t) = e^{-\mathrm{i}\lambda t}\mathbf{v}(\mathbf{x})$.

6. Numerical results

The algorithms described in Section 5 were implemented to compute wave functions of the two-coupled BEC [19] and the rotating BEC defined in the square, where the BiCGSTAB [31] was used as the linear solver. All computations were executed on a Pentium 4 computer using the MATLAB language. The accuracy tolerance of the linear solver and the stopping criterion in the Newton corrector of the continuation method is 10^{-10}. For the two-coupled BEC both a single peak solution and four boundary peak solutions on the four corners of the square can be obtained if the interaction of the two components is repulsive, and if the second continuation parameter λ_2 is properly chosen. We refer to [19] for the numerical results. The following examples describe the numerical results on the rotating BEC.

Example 1. Ground-state solutions of the rotating BEC with isotropic trapping potential. We studied wave functions of (1.6) defined on the square domain $\Omega = (-l, l) \times (-l, l)$ with $\varepsilon = 1$, $\mu = 100$ and $V(x, y) = \frac{x^2+y^2}{2}$. The equation was discretized by the centered difference approximations with uniform meshsize $h = \frac{1}{128}$. Figs. 1–2 show the superfluid densities of (1.6) with $\omega = 0.9$ and 0.95 at the target points of the first solution branches bifurcating at $(0, \lambda_1^*) \approx (0, 0.9557918)$ and $(0, \lambda_1^*) \approx (0, 0.9557909)$, where $\lambda = 3.6286285$ and $\lambda = 3.0570659$, respectively. Fig. 2 shows that the superfluid densities has 17 vortices, while Bao et al. [17] also obtained 17 vortices using a continuous normalized gradient flow (CNGF) method with a backward Euler finite difference (BEFD) discretization on the same domain, as well as the same angular velocity and the μ value. As we increased the angular velocity to $\omega = 0.999$, we obtained 20 vortices. The superfluid density shown in Fig. 3 strongly resembles the experimental result in [10]. Fig. 4 depicts the first solution branch of (1.6) bifurcating at $(0, \lambda^*) = (0, 1.0306184)$ with $\omega = 0.999$.

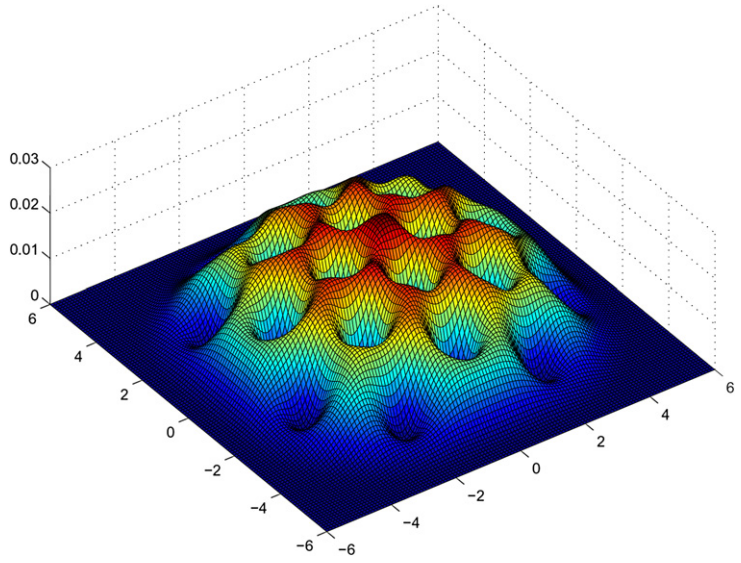

Fig. 2. The contour of the superfluid density $|\mathbf{v}|^2$ on the target point of the first solution branch of Eq. (1.6) with $l = 6$ and $\omega = 0.95$ at $\lambda = 3.0570659$.

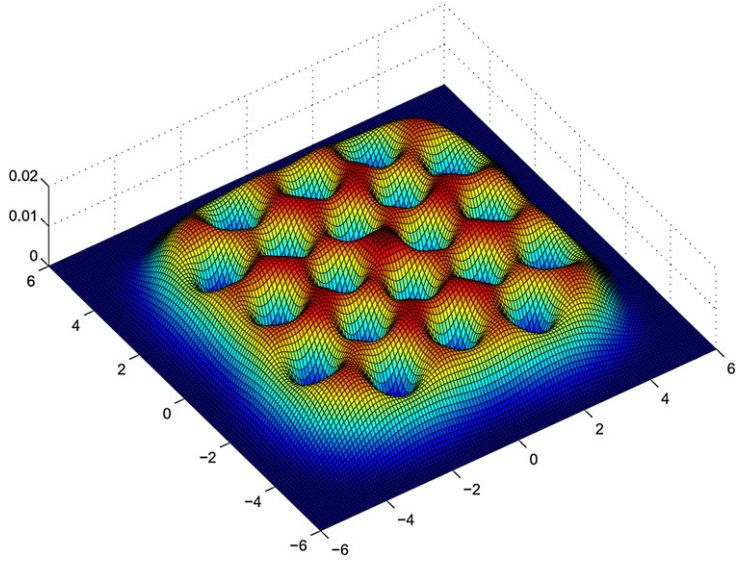

Fig. 3. The contour of the superfluid density $|\mathbf{v}|^2$ on the target point of the first solution branch of Eq. (1.6) with $l = 6$ and $\omega = 0.999$ at $\lambda = 2.3568152$.

Example 2. Excited state solutions of the rotating BEC with isotropic trapping potential. We used the same data as in Example 1. Nontrivial solution curves bifurcating at $(0, \lambda^*)$ with $6 < \lambda^* < 8$ were numerically traced. Fig. 5 shows how the superfluid densities on the solution branches of (1.6) vary with respect to the dimension $l = 2, 3, 4, 5$, where the angular velocity is $\omega = 0.1$. Fig. 6 displays the solution branches of (1.6) with $l = 2, 3, 4, 5$ and $\omega = 0.1$. Fig. 7 shows the superfluid densities of (1.6) with $l = 6$ and $\omega = 0.1$, 0.5 and 0.9, respectively.

Example 3. Ground-state solutions of the rotating BEC with nonisotropic trapping potential. We chose $V(\mathbf{x}) = \frac{1}{2}(x^2 + 2y^2)$ with $\varepsilon = 1$, $\mu = 100$ and $l = 6$. In this case, the first energy level is also twofold degenerate. We traced the first solution branches bifurcating at $(0, \lambda^*) = (0, 1.1334578)$ and $(0, 1.1342566)$ with $\omega = 0.9$ and 0.999, respectively. The target points are located at $\lambda = 5.3028822$ and $\lambda = 4.3386526$, respectively. Fig. 8 shows the former has eight vortices, and the latter six vortices.

7. Conclusion

In this paper, we have described a mesh refinement continuation algorithm for computing peak solutions of certain reaction-diffusion systems, including the GPE. Based on the discussions given in Sections 2–5, we may conclude that the numerical methods described in this paper have the following advantages: (1) Instead of using imaginary time evolution to minimize the energy

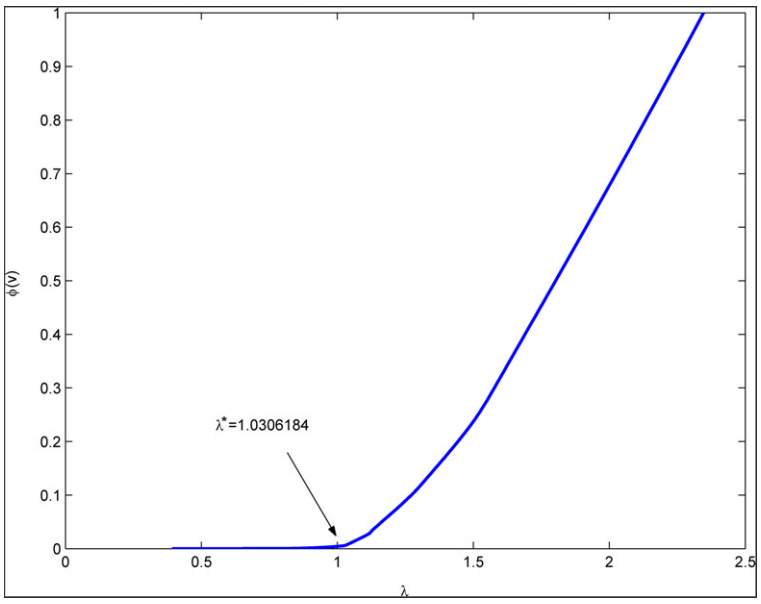

Fig. 4. The first solution branch of Eq. (1.6) bifurcating at $(0, \lambda^*) = (0, 1.0306184)$ with $l = 6$ and $\omega = 0.999$, $\phi(\mathbf{v})$ denotes the mass of the BEC.

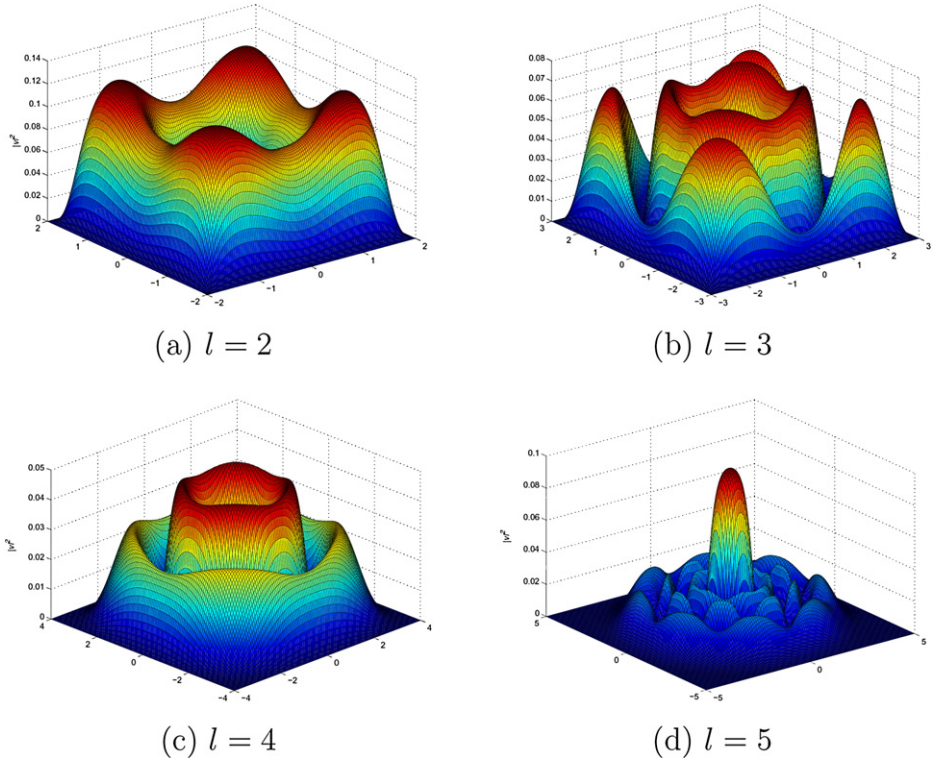

Fig. 5. The contours of the superfluid densities $|\mathbf{v}|^2$ on the target point of the solution branches of Eq. (1.6) with $\omega = 0.1$ and $l = 2, 3, 4, 5$, respectively.

functional for the ground-state of the GPE, we solve the associated stationary state nonlinear eigenvalue problem using numerical continuation methods. Note that we treat the total energy of the system as the continuation parameter, and the energy information of the SEP is fully exploited. Moreover, the numerical continuation method can easily compute excited states of the system. However, the former deals with the energy functional where the total energy is implicitly defined on the wave function. From the physical point of view, certainly our numerical methods give a more intuitive way to compute energy levels of the GPE. (2) In general, it takes at most three iterations for the Newton iteration to converge at each continuation step, which is quite inexpensive when the algorithm is implemented on the coarse grid. However, the imaginary time evolution has to be executed on the same grid level.

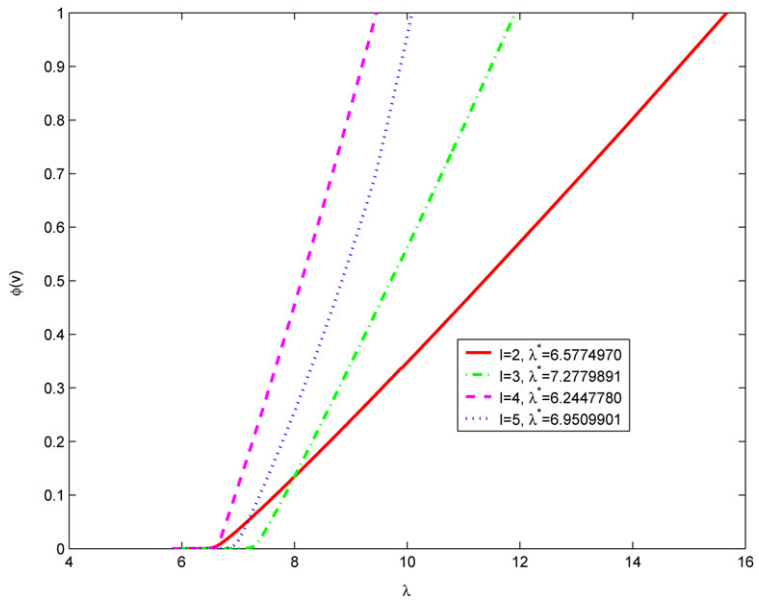

Fig. 6. The solution branches of Eq. (1.6) with $l = 2, 3, 4, 5$ and $\omega = 0.1$, $\phi(\mathbf{v})$ denotes the mass of the BEC.

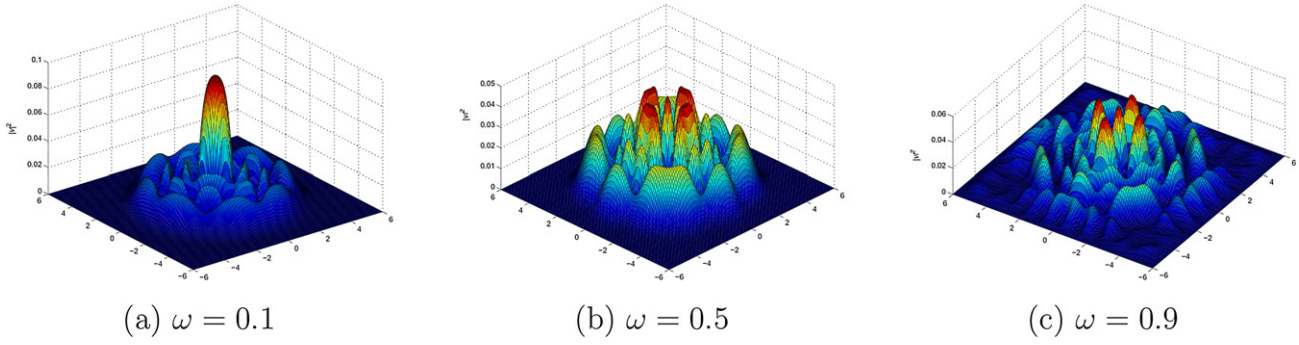

Fig. 7. The contours of the superfluid densities $|\mathbf{v}|^2$ on the target point of the other solution branches of Eq. (1.6) with $l = 6$ and $\omega = 0.1, 0.5, 0.9$, respectively.

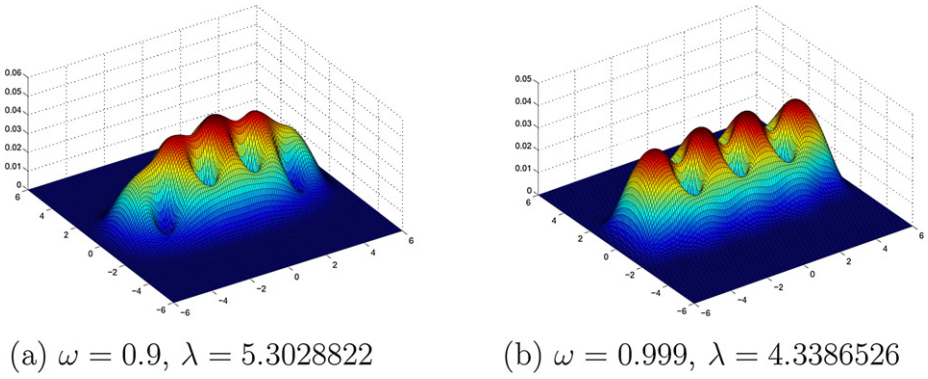

Fig. 8. The contours of the superfluid densities $|\mathbf{v}|^2$ on the target point of the first solution branches of Eq. (1.6) bifurcating at $(0, \lambda^*) = (0, 1.1334578)$ and $(0, 1.1342566)$ with $V(\mathbf{x}) = \frac{1}{2}(x^2 + 2y^2)$ and $\omega = 0.9$ at $\lambda = 5.3028822$, and $\omega = 0.999$ at $\lambda = 4.3386526$, respectively.

The energy levels of the rotating BEC have been extensively investigated with various angular velocities on various length scales of the domain. Our numerical results show that when $\Omega = (-6, 6) \times (-6, 6)$ and $\omega = 0.999$, the superfluid density of the ground-state solution, namely, the target point on first solution branch of the rotating GPE with isotropic trapping potential strongly resembles the figure shown in [10]. As we increased the domain to $\Omega = (-7, 7) \times (-7, 7)$, we still got the same size of vortex contour as shown in Fig. 4, which might explain that the core size of a quantized vortex is invariant. The superfluid densities we have obtained on the other solution branches of the rotating BEC, to the best of our knowledge, have never shown up in the literatures.

Acknowledgements

We would like to thank the two referees for their valuable comments that have improved the original version of this paper. We also thank Prof. W.-W. Lin of National Tsing Hua University, Taiwan, for showing us the paper of V. Mehrmann and D. Watkins.

References

[1] M.H. Anderson, J.R. Ensher, M.R. Matthews, C.E. Wieman, E.A. Cornell, Science 269 (1995) 198.
[2] D.A. Butts, D.S. Rokhsar, Nature 397 (1999) 327.
[3] M.R. Matthews, B.P. Anderson, P.C. Halian, D.S. Hall, C.E. Wieman, E.A. Cornell, Phys. Rev. Lett. 83 (1999) 2498.
[4] E.P. Gross, Nuovo Cimento 20 (1961) 454.
[5] L. Pitaevskii, Soviet Phys. JETP 13 (1961) 451.
[6] A.L. Fetter, A.A. Svidzinski, J. Phys. Condens. Matter 13 (2001) R135.
[7] K.W. Madison, F. Chevy, W. Wohlleben, J. Dalibard, Phys. Rev. Lett. 84 (2000) 806.
[8] C. Raman, J.R. Abo-Shaeer, J.M. Vogels, K. Xu, W. Ketterle, Phys. Rev. Lett. 87 (2001) 210402.
[9] P. Rosenbuch, V. Bretin, J. Dalibard, Phys. Rev. Lett. 89 (2002) 200403.
[10] J.R. Anglin, W. Ketterle, Nature 416 (2002) 211.
[11] J.J. García-Ripoll, V.M. Pérez-García, Phys. Rev. A 60 (1999) 4864.
[12] J.J. García-Ripoll, V.M. Pérez-García, Phys. Rev. A 63 (2001) 041603.
[13] J.J. García-Ripoll, V.M. Pérez-García, Phys. Rev. A 64 (2001) 053611.
[14] J.J. García-Ripoll, V.M. Pérez-García, SIAM J. Sci. Comput. 23 (2001) 1316.
[15] A. Aftalion, T. Riviere, Phys. Rev. A 64 (2001) 043611.
[16] A. Aftalion, Q. Du, Phys. Rev. A 64 (2001) 063603.
[17] W. Bao, H. Wang, P.A. Markowich, Comm. Math. Sci. 3 (2005) 57.
[18] S.A. Chin, E. Krotscheck, Phys. Rev. E 72 (2005) 036705.
[19] S.-L. Chang, C.-S. Chien, Inter. J. Bifurcation Chaos 17 (2007) 641.
[20] S.-L. Chang, C.-S. Chien, B.-W. Jeng, SIAM J. Sci. Comput. 27 (2007) 509.
[21] S.-L. Chang, C.-S. Chien, B.-W. Jeng, J. Comput. Phys., in press.
[22] W. Bao, D. Jaksch, P.A. Markowich, J. Comput. Phys. 187 (2003) 318.
[23] R.B. Bank, T.F. Chan, SIAM J. Sci. Stat. Comput. 7 (1986) 540.
[24] C. Gui, J. Wei, J. Differential Equations 158 (1999) 1.
[25] C. Gui, J. Wei, M. Winter, Ann. Inst. H. Poincaré Anal. Non Linéare 17 (2000) 47.
[26] V. Mehrmann, D. Watkins, SIAM J. Sci. Comput. 22 (2001) 1905.
[27] Z.-C. Li, T. Yamamoto, Q. Fang, J. Comput. Appl. Math. 156 (2003) 307.
[28] S.-L. Chang, C.-S. Chien, Z.-C. Li, 2007, submitted for publication.
[29] D. Gottlieb, S. A Orszag, Numerical Analysis of Spectral Methods: Theory and Applications, SIAM–CBMS, Philadelphia, 1997.
[30] L.N. Trefethen, Spectral Methods in MATLAB, SIAM, Philadelphia, 2000.
[31] H.A. van der Vorst, SIAM J. Sci. Stat. Comput. 13 (1992) 631.